TE dependent Diffusion Imaging (TEdDI) distinguishes between compartmental T_2 relaxation times

Jelle Veraart, **Dmitry S. Novikov**, and **Els Fieremans**

Center for Biomedical Imaging, Department of Radiology, New York University School of Medicine, NY, USA

Abstract

Biophysical modeling of macroscopic diffusion-weighted MRI (dMRI) signal in terms of microscopic cellular parameters holds the promise of quantifying the integrity of white matter. Unfortunately, even fairly simple multi-compartment models of proton diffusion in the white matter do not provide a unique, biophysically plausible solution. Here we report a nontrivial diffusion MRI signal dependence on echo time (T_E) in human white matter *in vivo*. We demonstrate that such T_E dependence originates from compartment-specific T_2 values and that it is a promising "orthogonal measure" able to break the degeneracy in parameter estimation, and to yield important relaxation metrics robustly. We thereby enable the precise estimation of the intra- and extra-axonal water T_2 relaxation values, which is precluded by a limited signal-to-noise ratio when using multi-echo relaxometry alone.

Keywords

transverse relaxation; diffusion; MRI; modeling

Introduction

Along with the appreciation of the clinical significance of the human white matter (WM), *in vivo* imaging of the human brain has been made possible by the development of Magnetic Resonance Imaging (MRI). MRI can visualize cubic millimeters of tissue, but that spatial resolution is still thousand times coarser than cell dimensions of microns. Nonetheless, MRI is capable of investigating cellular structure, by virtue of sensing the voxel-averaged mean squared displacement of diffusing proton-carrying molecules extending over a few μm and, as such, probing the hindrances and restrictions of the underlying cell architecture (Tanner, 1979; Callaghan et al., 1988; Cory and Garroway, 1990). Interpreting the macroscopic diffusion-weighted MRI (dMRI) signal in terms of microscopic cellular parameters *in vivo* is bound to be indirect, based on biophysical models of the MRI signal, but holds the promise of quantifying the integrity of the WM (e.g. Szafer et al., 1995; Stanisz et al., 1997;

Kroenke et al., 2004; Assaf and Basser, 2005; Jespersen et al., 2007; Assaf et al., 2008; Alexander et al., 2010; Jespersen et al., 2010; Yablonskiy and Sukstanskii, 2010; Fieremans et al., 2011; Zhang et al., 2012; Sotiropoulos et al., 2012; Jensen et al., 2016; Novikov et al., 2016b; Reisert et al., 2016; Kaden et al., 2016; Novikov et al., 2016a).

Compartmentalization, that is, the representation of MR signal as a sum of independent contributions from separate pools of water, corresponding to locally anisotropic intra- and extra-axonal spaces, underpins most biophysical MR models of proton diffusion in the WM. During the past decades, the community adopted the picture of restricted diffusion in an array of axons, represented by a collection of dispersed "sticks" (Kroenke et al., 2004; Jespersen et al., 2007; Veraart et al., 2016b; McKinnon et al., 2017) embedded in the extra-axonal water, whereas the contribution of myelin water is considered to be negligible due to its short T_2 (Vasilescu et al., 1978; Menon and Allen, 1991; Fischer et al., 1990; Mackay et al., 1994). Unfortunately, the ubiquitous presence of water in all cell types and the permeability of most tissue interfaces make it so far impossible to distinguish changes in dMRI caused by alterations in specific cell types, e.g. neurons or glia. Indeed, even fairly simple multi-compartment models accounting for the different compartments and cell types do provide more than one biophysically plausible solution (Jelescu et al., 2016a).

Similar multi-compartment models have been studied in the context of T_2 relaxometry. By exploring a wide range of echo times (T_E) during multi-echo acquisitions, one aims to quantify volume fractions of myelin water, intra-/extra-axonal water, and free water compartments (Meiboom and Gill, 1958; Mackay et al., 1994; Whittall et al., 1997). The inverse Laplace transform of the associated signal attenuation is expected to lead to a (multimodal) spectrum of T_2 values, which ideally reduces to a sum of delta peaks in case of superposed exponential decays. Unfortunately, the inverse Laplace transformation is ill-posed and, as such, unstable to small fluctuations in the measured data (Epstein and Schotland, 2008). Therefore, despite being a promising technique to quantify myelin water fractions, it has been shown that limited SNR precludes resolving the intra- and extra-axonal water peak using multi-echo relaxometry alone (Stanisz and Henkelman, 1998).

Differences in compartmental T_2 values would complicate the interpretation of diffusion models of white matter. For example, it has been observed that one of the model parameters of interest, i.e. the intra-axonal water fraction shows T_E-dependency (Buckley et al., 1999; De Santis et al., 2016). We will refer to the T_2-weighted intra-axonal water fraction as f(T_E). The T_E dependency of biophysically meaningful parameters not only hampers inter-study comparison, but it also restricts the validation of biophysical models using histology.

In this work, we evaluate the dMRI signal dependence on T_E in the human brain *in vivo*. We demonstrate empirically that exploiting such T_E dependence by incorporating a compartmental T_2 decay into biophysical modeling is a promising way to break the degeneracy in dMRI parameter estimation, and to yield compartmental relaxation metrics robustly and specifically. The specific assignment of nerve water T_2 components by simultaneously considering compartmental diffusion and transverse relaxation properties was already studied by Beaulieu et al. (1998) and Peled et al. (1999) in myelinated nerves of the garfish and frog sciatic nerve tissue, respectively. Despite some discrepancies (e.g. Kim

et al., 2017), more and more evidence is given for the T_2 relaxation time constants of intra- and extra-axonal water to be different from each other with the T_2 of the intra-axonal water component being the larger one (Peled et al., 1999; Wachowicz and Snyder, 2002; Dortch et al., 2010; Bonilla and Snyder, 2007); see also Discussion.

Our combined diffusion and relaxation approach is inspired by the vast literature on multidimensional methods of nuclear magnetic resonance (NMR) spectroscopy for the study of porous media, e.g. Diffusion-Relaxation Correlation Spectroscopy (DR-COSY) (Hürlimann et al., 2002; Hürlimann and Venkataramanan, 2002; Callaghan et al., 2003; Galvosas et al., 2007; Godefroy and Callaghan, 2003; Bernin and Topgaard, 2013). DRCOSY is a 2D NMR spectroscopic method that encodes diffusion and relaxation parameters jointly, and substantially improves the ability to distinguish different compartments. Clinical MR application of the technique were lacking due the associated cost in terms of data acquisition. Recent work of Benjamini and Basser (2016) and Kim et al. (2017) extended the spatially non-resolved method to an imaging technique by applying physical or spatial constraints, respectively. Benjamini and Basser (2016) proposed to use a priori information from the 1D projections of spectra to reconstruct the 2D spectrum. Because those marginal distributions provide physical constraints on the reconstruction of the 2D spectrum, the data requirements can be highly reduced in comparison with conventional 2D approaches.

In line with the spectroscopic approaches, we also aim to (a) resolve the different T_2 and diffusion compartments robustly, while (b) maintaining clinical feasibility by minimizing scan requirements. However, our methods is fundamentally different as we rely on a biophysical model to extract diffusion and relaxation parameters from a pre-defined set of compartments. By doing so, we reduce the number of parameters to be estimated, thereby increasing the precision of the parameter estimators and achieving a specific assignment of the compartments. Moreover, by adopting rotationally-invariant non-Gaussian basis functions to describe the underlying diffusion process in anisotropic neuronal compartments (Novikov et al., 2016b; Reisert et al., 2016), we can parameterize the non-Gaussianity of each compartment due to axonal dispersion more accurately than spectroscopic methods that rely on exponential basis functions.

1. Materials and Methods

1.1. Model assumptions—We here adopt a widely used two-compartment biophysical model of water inside narrow impermeable *sticks* (e.g. Jespersen et al., 2007), embedded in an extra-cellular matrix. The *stick* compartment – "intra-axonal space" – is assumed to represent axons (and possibly glial processes) inside which diffusion is locally one-dimensional. The second compartment – "extra-axonal space" – covers an effective connective tissue space inside which diffusion of water molecules is assumed to be hindered. The exchange between intra- and extra-axonal water is assumed to be negligible at the time scales of the measurements.

Stanisz et al. (1997) suggested to include an additional isotropically restricted compartment to represent stationary water, e.g. protons trapped glial cells. Others stated that glial water can be considered part of the effective extra-axonal space because glia cells might be in fast

exchange with the extra-axonal space due to the presence of aquaporin water channels (Arcienega et al., 2010; Nielsen et al., 1997; Nilsson et al., 2013; Pfeuffer et al., 1998). This hypothesis has recently been questioned by Yang et al. (2017). Nonetheless, after studying the functional form of the diffusion-weighted signal decay at b-values up to 10 ms/μm^2, we concluded that the signal fraction of such an isotropically restricted compartment is not significant given clinically relevant diffusion times (Veraart et al., 2016b). This conclusion is in agreement with Dhital et al. (2015), who observed a nearly monoexponential decay of the isotropically weighted diffusion data. Therefore, we here omit such a third diffusion compartment.

1.2. TEdDI—We extend the two-compartment model of diffusion in white matter by including the compartment-specific T_2-relaxation parameterized by T_2^a and T_2^e for the intra- and extra-axonal compartments, respectively, following the notation of Novikov et al. (2016b):

$$S_{\widehat{\mathbf{g}}}(b, T_E) = S(0,0) \cdot \int_{|\widehat{\mathbf{n}}| = 1} d\widehat{\mathbf{n}} \mathscr{P}(\widehat{\mathbf{n}}) \mathscr{K}(b, T_E, \widehat{\mathbf{g}} \cdot \widehat{\mathbf{n}}), \quad [1]$$

that is, a convolution between $\mathscr{P}(\widehat{\mathbf{n}})$, the axonal orientation distribution function (ODF), and

$$\mathscr{K}(b, T_E, \xi) = f_0 e^{-T_E/T_2^a - bD_a\xi^2} + (1 - f_0)e^{-T_E/T_2^e - bD_e^{\perp} - b(D_e^{\|} - D_e^{\perp})\xi^2}, \quad [2]$$

the signal response of an individual fiber fascicle; $\int d\widehat{\mathbf{n}} \mathscr{P}(\widehat{\mathbf{n}}) \equiv 1$. In Eq. 2, $S(0,0)$ denotes the proton density, b the diffusion-weighting strength, D_a the intra-axonal diffusivity, $D_e^{\|}$ and $D_e^{\perp}$ the axial and radial extra-axonal diffusivity, respectively, and $f_0 \equiv f(T_E)|_{T_E=0}$ the non-T_2-weighted intra-axonal water fraction that relates to the T_2-weighted, T_E-dependent relative fraction $f(T_E)$ as follows:

$$f(T_E) = \frac{f_0 e^{-T_E/T_2^a}}{f_0 e^{-T_E/T_2^a} + (1 - f_0)e^{-T_E/T_2^e}}. \quad [3]$$

We build upon the recently introduced rotationally invariant ("RotInv") framework (Novikov et al., 2016b; Reisert et al., 2016) that allows limiting the dimensionality of the parameter space by factoring out the ODF. Basically, we solve the following non-linear least squares estimation problem:

$$\hat{\mathbf{x}} = \arg \min_{\mathbf{x}} \sum_{l=0,2,\cdots}^{L} \|S_l(b, T_E) - p_l K_l(b, T_E; \mathbf{x})\|^2, \quad [4]$$

with $\hat{\mathbf{x}} = \left\{ S(0,0), f_0, D_a, D_e^{\parallel}, D_e^{\perp}, p_l, T_2^a, T_2^e \right\}$, the 8-tuple of estimated model parameters. The projections $K_l(b, T_E)$ of kernel $\mathscr{K}(b, T_E, \xi)$ onto Legendre polynomials include explicit T_E dependence. Note that the simultaneous estimation of diffusion and relaxation metrics requires that both the b-values and T_E vary during the acquisition. In Eq. [4], the rotational invariants

$$S_l^2(b, T_E) = \frac{1}{4\pi(2l+1)} \sum_{m=-l}^{l} |S_{lm}(b, T_E)|^2 \quad [5]$$

are computed from shells of the signal that are characterized by a unique b and T_E combination. The rotational invariants are constructed from the lth order, with a maximum of L, spherical harmonic coefficients $S_{lm}(b, T_E)$ that are estimated from the shelled data with b the shell radius (Tournier et al., 2004). The full ODF can be described by spherical harmonic coefficients p_{lm}, which constitute, e.g., 5, 14, or 27 parameters for $l = 2$, 4, or 6, respectively. Instead, for each order l, only a single rotationally invariant parameter p_l is derived from that representation:

$$p_l^2 = \frac{1}{4\pi(2l+1)} \sum_{m=-l}^{l} |p_{lm}|^2, \quad [6]$$

if $l > 0$; $p_0 \equiv 1$. Only even orders are considered because of the antipodally symmetric diffusion. Novikov et al. (2016b) and Reisert et al. (2016) showed recently that the dispersion angle of the ODF can be computed as $\cos^{-1}\sqrt{(2p_2+1)/3}$. The $L = 0$ rotational invariant K_0 has been studied before for a fixed T_E (Lasič et al., 2014; Jespersen et al., 2013; Kaden et al., 2016). Here we include invariants $K_{0,2}$ up to the 2$^{\text{nd}}$ order, thereby quantifying the axonal dispersion metric p_2, by solving Eq. 4 for $L = 2$. In contrast to earlier work of Kaden et al. (2016) and Zhang et al. (2012), we also lift constraints such as the tortuosity model (Sen and Basser, 2005) or fixed diffusivities (Alexander et al., 2010).

Combining the invariant K_l, up to the 2$^{\text{nd}}$ order, and an experimentally varying T_E constitutes a novel parameter estimation framework that we refer to as TEdDI, TE dependent Diffusion Imaging.

1.3. Simulations—We evaluate the accuracy and precision of TEdDI in a single-voxel simulation using 2500 noise realizations. The acquisition protocol matches the real data protocol. For underlying parameter values, we chose $f_0 = 0.45$, $D_a = 2.2 \, \mu\text{m}^2/\text{ms}$,

$D_e^{\parallel} = 2\,\mu\text{m}^2/\text{ms}$, $D_e^{\perp} = 0.5\,\mu\text{m}^2/\text{ms}$, $p_2 = 0.6$, $T_2^a = 90\,\text{ms}$, and $T_2^e = 60\,\text{ms}$ in agreement with our *in vivo* observations. The SNR for $S\,(0, 105\,\text{ms})$ is fixed to 50. We added Gaussian noise to exclude Rician noise biases from this analysis. Each fit was initiated with a single randomly chosen starting point, considering a biophysically plausible parameter range (such as $0 \leq f \leq 1$, $0 \leq p_2 \leq 1$, $0 \leq D \leq 3$ for all diffusivities, and $20 \leq T_2^a, T_2^e \leq 150$)

For each of the model parameters, the standard deviation across the different noise realizations was computed. We repeated this simulation for two diffusion-only representations, i.e. K_0 and $K_{0,2}$, with a fixed $T_E = 105\,\text{ms}$ to mimic realistic SNR values. The total number of diffusion-weighted images was kept constant by including more averages.

1.4. Data—Five healthy volunteers underwent imaging on a Siemens Prisma 3T MR scanner using a 64-channel receiver head coil with an EPI readout diffusion-weighted sequence. The subjects were scanned after obtaining informed consent as approved by our Institutional Review Board. Monopolar diffusion gradients were applied along 30 isotropically distributed directions for $b = 0.5, 1, 2, 3$, and $4\,\text{ms}/\mu\text{m}^2$. This diffusion protocol was repeated for $T_E = 69, 90, 120$, and $150\,\text{ms}$. However, due to scan limitations, the $b = 4\,\text{ms}/\mu\text{m}^2$ could not be acquired for $T_E = 69\,\text{ms}$. The diffusion time was not fixed during the acquisition: $\delta/\Delta = 20/35$ and $59/75\,\text{ms}$ for $T_E = 69$, and $150\,\text{ms}$, respectively. Additionally, 50 non-diffusion-weighted images, $b = 0$, were acquired with 11 different T_E's, which were equidistantly distributed between 55 and 145 ms. The following imaging parameters were kept constant: $T_R = 4000\,\text{ms}$, bandwidth: 2470 Hz/pixel, matrix: 88×88, NEX: 1, in-plane resolution: $2.5 \times 2.5\,\text{mm}^2$, slice thickness: 2.5 mm, slices: 50, parallel imaging: GRAPPA with acceleration factor 2, reconstructed using the adaptive combine algorithm to ensure Rician data distribution, multiband acceleration with factor 2, and no partial Fourier. The total scan time per volunteer was 60 minutes.

1.5. Data processing—First, we strongly reduced the noise in the data and we estimated the noise map by exploiting the inherent redundancy in diffusion MRI data for each T_E separately (Veraart et al., 2016a,c). The positive signal bias, inherent to low-SNR magnitude MR data, was removed by using the method of moments, where the denoised signal was used as a proxy for the Rician expectation value (Gudbjartsson and Patz, 1995). Denoised and Rician bias corrected images were subsequently corrected for Gibbs ringing (Kellner et al., 2015), geometric eddy current distortions and subject motion (Andersson and Sotiropoulos, 2015).

Second, for each T_E specific subset of the dMRI data, we estimated the fractional anisotropy (FA) and mean diffusvity (MD) using diffusion kurtosis imaging (DKI) (Jensen et al., 2005) (we excluded all $b > 2\,\text{ms}/\mu\text{m}^2$ for the DKI analysis), and $f(T_E)$ using RotInv up to the second order, $K_{0,2}$. For the latter, we initiated the fit by five randomly chosen starting points within biophysically or mathematically plausible bounds for each voxel.

Third, we estimated all TEdDI parameters $\hat{x}$ by solving Eq. 4 for each voxel by fitting the TEdDI model to all available dMRI data, including the different T_E's. We initialized each fit

using one random starting point sampled from following parameter ranges: 0 f 1, 0 p_2 1, 0 D 3 for all diffusivities, and $20 \leq T_2^a, T_2^e \leq 150$).

Finally, anatomical WM regions of interest were selected from the Johns Hopkins University WM atlas (Mori et al., 2005). The diffusion MR data, represented by the associated FA maps, were registered to the standard FA map in FSL (Smith et al., 2004) using FNIRT, the non-linear registration tool, after affine initialization of the registration. The inverse of the resulting warp fields were applied to the WM atlas to transform the ROI's into the subject spaces. The ten anatomical ROIs of our interest are the genu (GCC), splenium (SCC), and body (BCC) of the corpus callosum, anterior corona radiata (ACR), superior corona radiata (SCR), posterior corona radiata (PCR), the anterior and posterior limb of the internal capsule (ALIC and PLIC, respectively), the external capsule (EC), and the superior longitudinal fasciculus (SLF).

2. Results

2.1. T_E dependency of diffusion signal—In Fig. 1 we show the logarithm of $S(b, T_E)|_{b=0}$ as a function of T_E in the range of $T_E = 55$ to 150 ms, averaged over all voxels in the PLIC. The nonlinearity of $\log S(b, T_E)|_{b=0}$ uncovers non-monoexponential T_2 decay and indicates the existence of multiple T_2 components within this T_E range. At this point, we expect that CSF contributions can be disregarded due the imposed FA threshold of FA > 0.5 on the selected voxels. We quantified the nonlinearity of the log-signal decay by fitting a second order polynomial, $\alpha T_E^2 + \beta T_E + \gamma$, to the ROI-averaged log-signal. The 2nd order coefficient α was statistically larger than zero. Indeed, for all subjects, the 95% confidence interval for α excluded zero.

We also observe an increase of $f(T_E)$, as a function of T_E, ranging between 5 and 15%. For each T_E, the $f(T_E)$ was estimated from the associated dMRI data up to $b = 4\text{ms}/\mu\text{m}^2$ using RotInv up to the $L = 2$ and the median across all voxels within the PLIC is shown.

Finally, we show the average MD in the PLIC as a function of T_E. Interestingly, the T_E-dependency is less pronounced and less consistent across the subjects. Four subjects show a decrease in MD as a function of T_E that is significantly smaller in magnitude (2 to 4%) than the T_E-dependency of f. However, one subjects show an MD increase (up to 9%) that is slightly stronger than the increase observed for the corresponding f.

2.2. Simulations: noise propagation—In Fig. 2, scatter plots show the relation between each pair of parameters, estimated using K_0, $K_{0,2}$, and/or TEdDI. First, K_0 and $K_{0,2}$ are biased in the estimation of the f_0 due to its intrinsic T_2-weighting if the compartmental T_2 values are different. Second, the degeneracy and low precision in the estimation of the model parameters (Novikov et al., 2016b; Reisert et al., 2016), as observed for K_0 and $K_{0,2}$, is still present in TEdDI. However, most parameters, including all diffusion parameters, have similar or improved precision. Moreover, the T_2^a and D_a of the spurious family of solutions are outside a biophysically plausible range of values. Disregarding the estimates with implausible diffusion or T_2 metrics is effective for TEdDI, whereas such criteria are more

difficult to assign for K_0 and $K_{0,2}$. Indeed, the T_2 values are the better discriminator to distinguish between spurious and correct results of the fit. Here, we exclude all solutions with compartmental T_2 values outside the range 25 to 180 ms. The analysis of the omitted solutions revealed $D_a \quad 4 \ \mu m^2/ms$ in each case (not visible in Fig. 2).

In Fig. 3, we show the coefficients of variation (c_v), a unit-less metric computed as the ratio between the standard deviation and the reference value of the respective parameters. The results confirm that K_0 and $K_{0,2}$ suffer from poor precision in estimating the diffusion model parameters if no constraints are applied. However, it is shown that exploiting the T_E dependency often improves the precision in the estimation of the diffusion parameters. TEdDI also shows high precision in the estimation of both T_2 values, especially if the biophysically implausible solutions are trimmed away ("trimmed TEdDI"). To put these results in perspective: attempts to estimate the compartmental T_2 values using a constrained biexponential model, nonlinearly fitted to the $S(b = 0, T_E)$ only, resulted in a c_v that was an order of magnitude larger.

2.3. Experiments—In Fig. 4, we show the T_2^a and T_2^e maps as estimated with TEdDI. Although the maps are only shown for one subject, the histograms of compartmental T_2 values that cover all WM voxels are shown for all subjects in the bottom row. Next, we redid the fitting after imposing following hard constraint $T_2 \equiv T_2^a \equiv T_2^e$. The resulting map and histograms of T_2 are shown for comparison. However, most importantly, we compared the goodness-of-fit of the bi- and mono-exponential T_2 version of TEdDI using the corrected Akaike Information Criterion (AICc; Burnham and Anderson, 2002); AICc $= 2k + n \log (\|\varepsilon\|^2) + \frac{2k(k+1)}{n-k-1}$ with ε the vector of residuals after model fitting, n the number of T_2- and diffusion-weighted MR signals ($n = 52$ in this study) and k the number of model parameters, $k = 8$ if T_2^a and T_2^e are model parameters, while $k = 7$ if the constraint, that is, mono-exponential T_2 decay is imposed. We show the threshold map of the differences between the AICc for the constrained and unconstrained version to indicate which model is statistically more likely to describe the data better. An AICc difference of 2 or more is considered significant (Burnham and Anderson, 2002). With exception of CSF or CSF-dominated voxels, the unconstrained version of TEdDI, that is, the one including the compartmental T_2 values, fits the data statistically better. This observation is very consistent in all WM voxels.

Both the maps and histograms reflect that generally $T_2^a > T_2^e$. Despite some locally smooth maps, the compartmental T_2 values vary across different regions-of-interests (ROIs). A more quantitative and ROI specific overview of T_2^a and T_2^e is given in Fig. 5. The inter-subject differences in the estimation of T_2^a and T_2^e are smaller than the inter-ROI differences and inter-compartment differences.

We evaluated the potential impact of contributions from myelin water or intra-/extra-axonal water exchange by varying the minimal and maximal T_E, respectively (see Fig. 6). By gradually increasing the minimal T_E of both the non-diffusion weighted and diffusion-

weighted data from 55 to 85 ms, we do not see significant changes in the compartmental T_2 measurements (top row). Similarly, by enforcing a variable upper bound on the T_E's included in the analysis, from 125 to 155 ms, we again see a consistent estimation of T_2^a and T_2^e (bottom row). Therefore, we conclude that both effects can probably be neglected in the chosen T_E range.

Fig. 7 shows the maps of the diffusion parameters of a single subject, whereas Fig. 8 provides a more detailed ROI and inter subject analysis. Although a detailed study of those parameters and their reproducibility is beyond the scope of this study, we make following observations. First, the axonal water fraction f_0 is approximately 0.5, indicating that the intra-axonal and extra-axonal water fractions are almost equally represented in WM voxels if myelin water is excluded. Second, $D_a \neq D_e^{\parallel}$, but the the sign and magnitude of the differences between them vary across all subjects and ROIs. A systematic behavior is not observed in our data.

Discussion

In this work, empirical evidence is given for the T_2 relaxation time constants of intra- and extra-axonal water to be different, up to a factor of two, by simultaneously exploiting the transverse relaxation and diffusion properties of the different compartments. Although no consensus has been reached on the nature or origin of multiple T_2 components, our observation of $T_2^a > T_2^e$ is in agreement with earlier work that studied T_2 relaxometry in excised nerve tissue, as we discuss below.

T$_2$ relaxation

Despite a general trend to capture both extra- and intra-axonal water in the same distribution or peak of T_2 values using multi-echo relaxometry studies, Whittall et al. (1997) already showed that intra- and extracellular water might exhibit distinct T_2-values in white matter structures such as the PLIC. Such experiments are challenged by limited SNR or insufficient number of echoes to resolve the intra- and extra-axonal water peak. Nonetheless, in the past two decades, considerable evidence from several laboratories has been given to support the hypothesis that the T_2 relaxation time constants of intra- and extra-axonal water are different. A lack of T_E dependency of apparent diffusion coefficients precluded Beaulieu et al. (1998) from the specific interference of T_2 compartmentalization. However, Peled et al. (1999) observed a component with intermediate T_2 and unrestricted diffusion on a timescale of 100 ms and a neural component with long T_2 and restricted diffusion. The latter is consistent with intra-axonal water, whereas the former is compatible with an extracellular space. The abundance of collagen in the sciatic nerve has been hypothesized to be the origin of the fast relaxation of the extra-axonal water. Wachowicz and Snyder (2002) made a similar assignment by altering the molecular composition of water components of the amphibian peripheral nerve using paramagnetic agents.

Although the microscopic structure of peripheral nerve differs from that of WM, it could be anticipated that distinct peaks, corresponding to myelin water, extracellular water and axonal

water, should also be distinguishable in WM. However, it was only after the administration of Chromium in the rat WM and optic nerve that Dortch et al. (2010) were able to separate the compartmental T_2 peaks. Based on the postulation that the myelin sheath reduces the intra-axonal access of paramagnetic Chromium, resulting in smaller contrast-enhancement of intra-relative to extra-axonal water, the spectral component with the longest relaxation times is believed to be intra-axonal water. Bonilla and Snyder (2007) introduced cellular swelling in the rat optic nerve by bathing the nerves in a glutamate solution. They observed that the size of the slowest relaxing component increased and, as such, $T_2^a > T_2^e$.

The biophysical underpinnings of this finding are not yet well understood. The fast exchange of protons between either the intra- or extracellular space and the myelin sheath might be a contributing factor. The axonal membrane might slow down the exchange relative to the extra-axonal space, as such, the apparent T_2 values. Moreover, the larger surface-to-volume ratio in the extra-cellular space and the associated larger surface relaxation might contribute to the observation, but more experimental data is needed to support this hypothesis. Because factors such axonal packing and g-ratio determine the surface-to-volume ratio, we hypothesize TEdDI might provide sensitive, but not specific, biomarkers for such microstructural properties. Indeed, we expect that both a denser packing and higher g-ratio will increase the difference between the compartmental T_2 values.

Diffusion

Without being sensitive to myelin fraction, we measured a T_2 unweighted extra-/intra-axonal water fraction of approximately 50%. Hence, by assuming a myelin volume fraction of about 30% (Stanisz et al., 1999), we anticipate both an intra-and extra-axonal water fraction of ~35%. This result is in agreement with Tang et al. (1997), who reported a volume fraction of myelinated axons of 33% after studying age-related WM changes using stereological methods. Similarly, Jelescu et al. (2016b) reported myelinated axonal volume fraction in the murine GCC of 28–40% using electron microscopy. Note that it is not well established whether the intra-axonal water fraction captures both the myelinated and unmyelinated axons, or whether glial cells can be considered part of the extra-axonal space instead of having their own compartment. Targeted experiments that focus on unmyelinated nerve tissue might be necessary to evaluate the validity of the stick model, i.e. no exchange, for unmyelinated axons.

In agreement with our simulations, we notice anti-correlations between D_a and $D_e^{\parallel}$ when considering different ROI's across different subjects. Those correlations limit the reproducibility and interpretation of the individual parameters. Basically, this observation indicates that the model is too complex given the information encoded in the diffusion-weighted data. Reisert et al. (2016) already raised concerns about the number of independent parameters that can be extracted. However, instead of imposing constraints, we promote the addition of an orthogonal measurement, e.g., varying T_E in our case, using isotropically weighted diffusion MRI (Dhital et al., 2015) or qMAS (Eriksson et al., 2013), or exploring high b-values (Veraart et al., 2016b) to resolve the intrinsic correlations currently present in our data and to resolve the outliers we still observe in all the maps.

In agreement with earlier work, we only observe a small T_E-dependency of the mean diffusivity (Qin et al., 2009). Given two compartments, the trace of the diffusion tensor can be written as tr $(D(T_E)) = $ tr$(D_e) + f(T_E)$ (tr$(D_a) - $ tr(D_e)), with tr$(D_a) = D_a$ and tr$(D_e) = D_e^{\parallel} + 2D_e^{\perp}$ the trace of the intra- and extra-axonal tensor, respectively. Any T_E-dependency of f is scaled by the difference between the compartmental traces. However, Dhital et al. (2015) demonstrated that the traces of the intra- and extra-axonal compartments are similar when applying isotropically diffusion weighting and observing low kurtoses in the WM. Our results lean towards the same observation. The sign of the nearly zero difference was not consistent across the subjects though; hence the different, yet subtle, trends of tr $(D(T_E))$.

Limitations

In addition to the model assumption discussed earlier, we assume that different T_2 components can be associated with the same two microstructural compartments, which were initially defined by their mesoscopic diffusion properties. However, one must be aware that the role of exchange between the intra- and extra-axonal compartments might be different for proton diffusion and relaxation. Empirical evidence is given for water exchange between the intra- and extra-axonal compartment to be negligible during a diffusion time of ~50 ms (Veraart et al., 2016b). However, with T_E's up to 150 ms, one cannot exclude exchange as a potential confounding factor in the compartmentalization of T_2 weighted signal Yang et al. (2017). Currently, we lack accurate water exchange times in white matter to predict the magnitude of the effect (Lampinen et al., 2017). Nonetheless, by reducing the maximal T_E in our study to 120 ms, we did not observe significant effects. Therefore, we believe that the role of water exchange is minimal.

Potential biases introduced by fixing the number of compartments are very visible in regions that exhibit partial voluming with the CSF. Elevated T_2 values and diffusivities are a hallmark of CSF contamination. Therefore it was important to choose our ROI's conservatively by imposing an FA threshold of 0.5 on top of the automated, atlas-based ROI delineation. The overall effect of myelin contribution on the estimation of the compartmental T_2 values might be more subtle, yet significant, if the minimal T_E is not chosen with caution. Myelin water is characterized by a T_2 relaxation time of $10 - 20$ ms (Vasilescu et al., 1978; Menon and Allen, 1991; Fischer et al., 1990; Mackay et al., 1994; Alonso-Ortiz et al., 2015; Stanisz et al., 1999) and therefore, we advise not to use $T_E < 50$ ms. Nonetheless, it must be noted that slightly higher T_2 relaxation times for myelin have been reported. For example, Beaulieu et al. (1998) reported a T_2 for myelin water of 40 ms). Hence our advised minimal T_E might need to be adjusted if more conclusive T_2 measurement of myelin water appear (Zhang et al., 2015).

The lower bound on T_E might be a limiting factor in light of recent technical advancements, i.e. strong gradient systems, that enable exploring a wider T_E range. In-line with many estimation problems, a wider T_E range will boost precision of associated parameter estimators. However, myelin water contributions might jeopardize the accuracy of the measurements, unless the myelin compartment is added to the model accordingly, together with its diffusive properties. To make sure that myelin did not contribute significantly to our

findings, we varied the minimal T_E included in our analysis and found no significant effect by stepping from a minimal T_E of 55 to 85 ms.

Another potential confounding factor in our study is that the diffusion time varies across the different T_E's. Although diffusion time dependency of diffusion MR has been observed before (Fieremans et al., 2016) in human white matter, we assume that its contribution to our findings might be minimal because of the minimal changes observed when using different T_E ranges. We will explore the effect of diffusion time dependency on TEdDI in more detail as part of future work.

Optimal design

The data analyzed in this study is unusually rich because of a dense sampling in both b and T_E. Of course, the one-hour-long protocol has limited value in a clinical setting. The effect of T_E range and maximal b-value in terms of precision must be better understood before a clinical protocol can be designed. However, in comparison with previous optimal design studies, we added an extra layer of complexity, that is, the T_E may vary across the b-shells. Indeed, more and more, diffusion MR data tend to include multiple b-shells, with an increasing trend towards high b exploration. Nowadays, the T_E is kept constant for all b-shells, and its value is chosen in order to accommodate the diffusion-encoding gradients needed to achieve the highest b-value. Obviously, one suffers from signal loss through T_2 relaxation and this is a high price to pay for the lower b-values that would allow shorter T_E's. In that respect, the ideal TEdDI protocol is likely to be more optimal in terms of SNR for the lower b-values.

The observation that $T_2^a > T_2^e$ has some practical implications for protocol design. For example, tractography might benefit from longer T_E, despite its intrinsically lower SNR. Indeed, the signal will be more dominated by the intra-axonal signal at longer T_E and we hypothesize that the resulting signal orientation distribution function might be sharper in that case (Jensen et al., 2016). Moreover, the observed heterogeneity across different ROI's put an upper bound on the accuracy of methods that rely on prior knowledge or globally fixing parameter (Zhang et al., 2012; Kaden et al., 2016), not to mention kernel-driven diffusion or tractography methods such as constrained spherical deconvolution (Tournier et al., 2004, 2007). Instead, we advocate for tractography based on signal deconvolutions with a locally parameterized microstructural kernel (Jespersen et al., 2007; Reisert et al., 2014; Kaden et al., 2015; Reisert et al., 2016; Novikov et al., 2016b).

Conclusion

Varying the T_E of a diffusion-weighted MR experiment enables the simultaneous estimation of compartmental diffusivities and T_2 values. We provide experimental evidence for different T_2 values of intra- and extra-axonal water in the living human brain. Although the ROI-specific compartmental T_2 values may become useful parameters in studying WM microstructure, the heterogeneity and biophysical underpinnings of this phenomenon are not yet well understood. However, including compartmental T_2 values provides a promising avenue to lift the degeneracy of biophysical modeling of water diffusion in the brain.

Acknowledgments

References

Alexander DC, Hubbard PL, Hall MG, Moore EA, Ptito M, Parker GJ, Dyrby TB. Orientationally invariant indices of axon diameter and density from diffusion MRI. Neuroimage. 2010; 52(4):1374–1389. [PubMed: 20580932]

Alonso-Ortiz E, Levesque IR, Pike GB. MRI-based myelin water imaging: A technical review. Magnetic resonance in medicine. 2015; 73(1):70–81. [PubMed: 24604728]

Andersson JL, Sotiropoulos SN. Non-parametric representation and prediction of single-and multi-shell diffusion-weighted mri data using gaussian processes. NeuroImage. 2015; 122:166–176. [PubMed: 26236030]

Arcienega I, Brunet J, Bloch J, Badaut J. Cell locations for AQP1, AQP4 and 9 in the non-human primate brain. Neuroscience. 2010; 167(4):1103–1114. [PubMed: 20226845]

Assaf Y, Basser PJ. Composite hindered and restricted model of diffusion (CHARMED) MR imaging of the human brain. Neuroimage. 2005; 27(1):48–58. [PubMed: 15979342]

Assaf Y, Blumenfeld-Katzir T, Yovel Y, Basser PJ. AxCaliber: a method for measuring axon diameter distribution from diffusion MRI. Magnetic resonance in medicine. 2008; 59(6):1347–1354. [PubMed: 18506799]

Beaulieu C, Fenrich FR, Allen PS. Multicomponent water proton transverse relaxation and T2-discriminated water diffusion in myelinated and nonmyelinated nerve. Magnetic resonance imaging. 1998; 16(10):1201–1210. [PubMed: 9858277]

Benjamini D, Basser PJ. Use of marginal distributions constrained optimization (MADCO) for accelerated 2D MRI relaxometry and diffusometry. Journal of Magnetic Resonance. 2016; 271:40–45. [PubMed: 27543810]

Bernin D, Topgaard D. Nmr diffusion and relaxation correlation methods: New insights in heterogeneous materials. Current opinion in colloid Interface science. 2013; 18(3):166–172.

Bonilla I, Snyder RE. Transverse relaxation in rat optic nerve. NMR in Biomedicine. 2007; 20(2):113–120. [PubMed: 16998953]

Buckley DL, Bui JD, Phillips MI, Zelles T, Inglis BA, Plant HD, Blackband SJ. The effect of ouabain on water diffusion in the rat hippocampal slice measured by high resolution NMR imaging. Magnetic resonance in medicine. 1999; 41(1):137–142. [PubMed: 10025621]

Burnham KP, Anderson DR. Model Selection and Multi-model Inference. Springer; New York: 2002. Information and Likelihood Theory: A Basis for Model Selection and Inference; 49–97. URL

Callaghan P, Eccles C, Xia Y. NMR microscopy of dynamic displacements: k-space and q-space imaging. Journal of Physics E: Scientific Instruments. 1988; 21(8):820.

Callaghan P, Godefroy S, Ryland B. Use of the second dimension in PGSE NMR studies of porous media. Magnetic resonance imaging. 2003; 21(3):243–248. [PubMed: 12850714]

Cory D, Garroway A. Measurement of translational displacement probabilities by NMR: an indicator of compartmentation. Magnetic resonance in medicine. 1990; 14(3):435–444. [PubMed: 2355827]

De Santis S, Assaf Y, Jones D. The influence of t2 relaxation in measuring the restricted volume fraction in diffusion MRI. Proceedings of the International Society for Magnetic Resonance in Medicine. 2016; 24:1998.

Dhital B, Kellner E, Reisert M, Kiselev VG. Isotropic diffusion weighting provides insight on diffusion compartments in human brain white matter in vivo. Proceedings of the International Society for Magnetic Resonance in Medicine. 2015; 23:2788.

Dortch RD, Apker GA, Valentine WM, Lai B, Does MD. Compartment-specific enhancement of white matter and nerve ex vivo using chromium. Magnetic resonance in medicine. 2010; 64(3):688–697. [PubMed: 20806376]

Epstein CL, Schotland J. The bad truth about Laplace's transform. SIAM review. 2008; 50(3):504–520.

Eriksson S, Lasic S, Topgaard D. Isotropic diffusion weighting in PGSE NMR by magic-angle spinning of the q-vector. Journal of Magnetic Resonance. 2013; 226:13–18. [PubMed: 23178533]

Fieremans E, Burcaw LM, Lee HH, Lemberskiy G, Veraart J, Novikov DS. In vivo observation and biophysical interpretation of time-dependent diffusion in human white matter. Neuroimage. Jan. 2016 129:414–427. [PubMed: 26804782]

Fieremans E, Jensen JH, Helpern JA. White matter characterization with diffusional kurtosis imaging. Neuroimage. 2011; 58(1):177–188. [PubMed: 21699989]

Fischer HW, Rinck PA, van Haverbeke Y, Muller RN. Nuclear relaxation of human brain gray and white matter: analysis of field dependence and implications for MRI. Magnetic resonance in medicine. 1990; 16(2):317–334. [PubMed: 2266850]

Galvosas P, Qiao Y, Schönhoff M, Callaghan PT. On the use of 2D correlation and exchange NMR spectroscopy in organic porous materials. Magnetic resonance imaging. 2007; 25(4):497–500. [PubMed: 17466772]

Godefroy S, Callaghan P. 2d relaxation/diffusion correlations in porous media. Magnetic Resonance Imaging. 2003; 21(3):381–383. [PubMed: 12850739]

Gudbjartsson H, Patz S. The Rician distribution of noisy MRI data. Magnetic resonance in medicine. 1995; 34(6):910–914. [PubMed: 8598820]

Hürlimann M, Venkataramanan L. Quantitative measurement of two-dimensional distribution functions of diffusion and relaxation in grossly inhomogeneous fields. Journal of Magnetic Resonance. 2002; 157(1):31–42. [PubMed: 12202130]

Hürlimann M, Venkataramanan L, Flaum C. The diffusion–spin relaxation time distribution function as an experimental probe to characterize fluid mixtures in porous media. The Journal of chemical physics. 2002; 117(22):10223–10232.

Jelescu IO, Veraart J, Fieremans E, Novikov DS. Degeneracy in model parameter estimation for multi-compartmental diffusion in neuronal tissue. NMR in Biomedicine. 2016a; 29(1):33–47. [PubMed: 26615981]

Jelescu IO, Zurek M, Winters KV, Veraart J, Rajaratnam A, Kim NS, Babb JS, Shepherd TM, Novikov DS, Kim SG, et al. In vivo quantification of demyelination and recovery using compartment-specific diffusion mri metrics validated by electron microscopy. NeuroImage. 2016b; 132:104–114. [PubMed: 26876473]

Jensen JH, Glenn GR, Helpern JA. Fiber ball imaging. NeuroImage. 2016; 124:824–833. [PubMed: 26432187]

Jensen JH, Helpern JA, Ramani A, Lu H, Kaczynski K. Diffusional kurtosis imaging: The quantification of non-gaussian water diffusion by means of magnetic resonance imaging. Magnetic resonance in medicine. 2005; 53(6):1432–1440. [PubMed: 15906300]

Jespersen SN, Bjarkam CR, Nyengaard JR, Chakravarty MM, Hansen B, Vosegaard T, Ostergaard L, Yablonskiy D, Nielsen NC, Vestergaard-Poulsen P. Neurite density from magnetic resonance diffusion measurements at ultrahigh field: Comparison with light microscopy and electron microscopy. Neuroimage. Jan; 2010 49(1):205–216. [PubMed: 19732836]

Jespersen SN, Kroenke CD, Østergaard L, Ackerman JJ, Yablonskiy DA. Modeling dendrite density from magnetic resonance diffusion measurements. Neuroimage. 2007; 34(4):1473–1486. [PubMed: 17188901]

Jespersen SN, Lundell H, Sønderby CK, Dyrby TB. Orientationally invariant metrics of apparent compartment eccentricity from double pulsed field gradient diffusion experiments. NMR in Biomedicine. 2013; 26(12):1647–1662. [PubMed: 24038641]

Kaden E, Kelm ND, Carson RP, Does MD, Alexander DC. Multi-compartment microscopic diffusion imaging. NeuroImage. 2016; 139:346–359. [PubMed: 27282476]

Kaden E, Kruggel F, Alexander DC. Quantitative mapping of the per-axon diffusion coefficients in brain white matter. Magnetic resonance in medicine. 2015; doi: 10.1002/mrm.25734

Kellner E, Dhital B, Kiselev VG, Reisert M. Gibbs-ringing artifact removal based on local subvoxel-shifts. Magnetic resonance in medicine. 2015; doi: 10.1002/mrm.26054

Kim D, Doyle EK, Wisnowski JL, Kim JH, Haldar JP. Diffusion-relaxation correlation spectroscopic imaging: A multidimensional approach for probing microstructure. Magnetic Resonance in Medicine. 2017

Kroenke CD, Ackerman JJ, Yablonskiy DA. On the nature of the NAA diffusion attenuated MR signal in the central nervous system. Magnetic resonance in medicine. 2004; 52(5):1052–1059. [PubMed: 15508157]

Lampinen B, Szczepankiewicz F, Westen D, Englund E, Sundgren CP, Lätt J, Sthlberg F, Nilsson M. Optimal experimental design for filter exchange imaging: apparent exchange rate measurements in the healthy brain and in intracranial tumors. Magnetic resonance in medicine. 2017; 77(3):1104–1114. [PubMed: 26968557]

Lasi S, Szczepankiewicz F, Eriksson S, Nilsson M, Topgaard D. Microanisotropy imaging: quantification of microscopic diffusion anisotropy and orientational order parameter by diffusion MRI with magic-angle spinning of the q-vector. Frontiers in Physics. 2014; 2:11.

Mackay A, Whittall K, Adler J, Li D, Paty D, Graeb D. In vivo visualization of myelin water in brain by magnetic resonance. Magnetic Resonance in Medicine. 1994; 31(6):673–677. [PubMed: 8057820]

McKinnon ET, Jensen JH, Glenn GR, Helpern JA. Dependence on b-value of the direction-averaged diffusion-weighted imaging signal in brain. Magnetic Resonance Imaging. 2017; 36:121–127. [PubMed: 27989904]

Meiboom S, Gill D. Modified spin-echo method for measuring nuclear relaxation times. Review of scientific instruments. 1958; 29(8):688–691.

Menon R, Allen P. Application of continuous relaxation time distributions to the fitting of data from model systmes and excised tissue. Magnetic resonance in medicine. 1991; 20(2):214–227. [PubMed: 1775048]

Mori S, Wakana S, Van Zijl PC, Nagae-Poetscher L. MRI atlas of human white matter. Elsevier; 2005.

Nielsen S, Nagelhus EA, Amiry-Moghaddam M, Bourque C, Agre P, Ottersen OP. Specialized membrane domains for water transport in glial cells: high-resolution immunogold cytochemistry of aquaporin-4 in rat brain. Journal of Neuroscience. 1997; 17(1):171–180. [PubMed: 8987746]

Nilsson M, Lätt J, van Westen D, Brockstedt S, Lasi S, Sthlberg F, Topgaard D. Noninvasive mapping of water diffusional exchange in the human brain using filter-exchange imaging. Magnetic resonance in medicine. 2013; 69(6):1572–1580.

Novikov DS, Jespersen SN, Kiselev VG, Fieremans E. Quantifying brain microstructure with diffusion mri: Theory and parameter estimation. Dec.2016a arXiv:1612.02059.

Novikov DS, Veraart J, Jelescu IO, Els F. Mapping orientational and microstructural metrics of neuronal integrity with in vivo diffusion MRI. Sep.2016b arXiv:1609.09144.

Peled S, Cory DG, Raymond SA, Kirschner DA, Jolesz FA. Water diffusion, T2, and compartmentation in frog sciatic nerve. Magnetic resonance in medicine. 1999; 42(5):911. [PubMed: 10542350]

Pfeuffer J, Flögel U, Dreher W, Leibfritz D. Restricted diffusion and exchange of intracellular water: theoretical modelling and diffusion time dependence of 1h nmr measurements on perfused glial cells. NMR in Biomedicine. 1998; 11(1):19–31. [PubMed: 9608585]

Qin W, Shui Yu C, Zhang F, Du XY, Jiang H, Xia Yan Y, Cheng Li K. Effects of echo time on diffusion quantification of brain white matter at 1.5 t and 3.0 t. Magnetic resonance in medicine. 2009; 61(4):755–760. [PubMed: 19191286]

Reisert M, Kellner E, Dhital B, Hennig J, Kiselev VG. Disentangling micro from mesostructure by diffusion MRI: A bayesian approach. NeuroImage. 2016; doi: 10.1016/j.neuroimage.2016.09.058

Reisert M, Kiselev VG, Dihtal B, Kellner E, Novikov D. Mesoft: unifying diffusion modelling and fiber tracking. International Conference on Medical Image Computing and Computer-Assisted Intervention; Springer; 2014. 201–208.

Sen PN, Basser PJ. A model for diffusion in white matter in the brain. Biophysical journal. 2005; 89(5):2927–2938. [PubMed: 16100258]

Smith SM, Jenkinson M, Woolrich MW, Beckmann CF, Behrens TE, Johansen-Berg H, Bannister PR, De Luca M, Drobnjak I, Flitney DE, et al. Advances in functional and structural MR image analysis and implementation as FSL. Neuroimage. 2004; 23:S208–S219. [PubMed: 15501092]

Sotiropoulos SN, Behrens TE, Jbabdi S. Ball and rackets: inferring fiber fanning from diffusion-weighted MRI. NeuroImage. 2012; 60(2):1412–1425. [PubMed: 22270351]

Stanisz G, Kecojevic A, Bronskill M, Henkelman R. Characterizing white matter with magnetization transfer and t2. Magnetic resonance in medicine. 1999; 42(6):1128–1136. [PubMed: 10571935]

Stanisz GJ, Henkelman RM. Diffusional anisotropy of T2 components in bovine optic nerve. Magnetic resonance in medicine. 1998; 40(3):405–410. [PubMed: 9727943]

Stanisz GJ, Wright GA, Henkelman RM, Szafer A. An analytical model of restricted diffusion in bovine optic nerve. Magnetic Resonance in Medicine. 1997; 37(1):103–111. [PubMed: 8978638]

Szafer A, Zhong J, Gore JC. Theoretical model for water diffusion in tissues. Magnetic resonance in medicine. 1995; 33(5):697–712. [PubMed: 7596275]

Tang Y, Nyengaard J, Pakkenberg B, Gundersen H. Age-induced white matter changes in the human brain: a stereological investigation. Neurobiology of aging. 1997; 18(6):609–615. [PubMed: 9461058]

Tanner J. Self diffusion of water in frog muscle. Biophysical journal. 1979; 28(1):107–116. [PubMed: 318065]

Tournier JD, Calamante F, Connelly A. Robust determination of the fibre orientation distribution in diffusion MRI: non-negativity constrained super-resolved spherical deconvolution. NeuroImage. 2007; 35(4):1459–1472. [PubMed: 17379540]

Tournier JD, Calamante F, Gadian DG, Connelly A. Direct estimation of the fiber orientation density function from diffusion-weighted MRI data using spherical deconvolution. NeuroImage. 2004; 23(3):1176–1185. [PubMed: 15528117]

Vasilescu V, Katona E, Simplaceanu V, Demco D. Water compartments in the myelinated nerve. III. Pulsed NMR result. Cellular and Molecular Life Sciences. 1978; 34(11):1443–1444.

Veraart J, Fieremans E, Novikov DS. Diffusion MRI noise mapping using random matrix theory. Magnetic resonance in medicine. 2016a; doi: 10.1002/mrm.26059

Veraart J, Fieremans E, Novikov DS. Universal power-law scaling of water diffusion in human brain defines what we see with MRI. Sep.2016b arXiv:1609.09145.

Veraart J, Novikov DS, Christiaens D, Ades-Aron B, Sijbers J, Fieremans E. Denoising of diffusion MRI using random matrix theory. NeuroImage. 2016c; 142:394–406. [PubMed: 27523449]

Wachowicz K, Snyder RE. Assignment of the T2 components of amphibian peripheral nerve to their microanatomical compartments. Magnetic resonance in medicine. 2002; 47(2):239–245. [PubMed: 11810666]

Whittall KP, Mackay AL, Graeb DA, Nugent RA, Li DK, Paty DW. In vivo measurement of T2 distributions and water contents in normal human brain. Magnetic Resonance in Medicine. 1997; 37(1):34–43. [PubMed: 8978630]

Yablonskiy DA, Sukstanskii AL. Theoretical models of the diffusion weighted MR signal. NMR in Biomedicine. 2010; 23(7):661–681. [PubMed: 20886562]

Yang DM, Huettner JE, Bretthorst GL, Neil JJ, Garbow JR, Ackerman JJ. Intracellular water preexchange lifetime in neurons and astrocytes. Magnetic Resonance in Medicine. 2017. n/a–n/a. URL

Zhang H, Schneider T, Wheeler-Kingshott CA, Alexander DC. NODDI: practical in vivo neurite orientation dispersion and density imaging of the human brain. Neuroimage. 2012; 61(4):1000–1016. [PubMed: 22484410]

Zhang J, Kolind SH, Laule C, MacKay AL. Comparison of myelin water fraction from multiecho t2 decay curve and steady-state methods. Magnetic resonance in medicine. 2015; 73(1):223–232. [PubMed: 24515972]
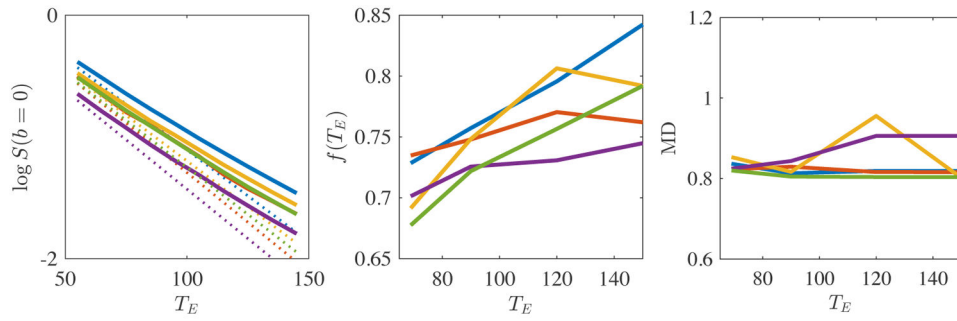
Figure 1.
The PLIC-averaged logarithm of non-diffusion weighted signal $S(b=0, T_E)$ (left), the corresponding estimated T_2-weighted axonal water fraction $f(T_E)$ (middle), and mean diffusivity (MD) are shown as a function of T_E for each subject (different colors). The linear approximation of the log signal decay is shown in dashed lines. Despite a non-consistent T_E-dependency of MD across subjects, the statistically significant non-monoexponential signal decay and monotonically increasing $f(T_E)$ support the hypothesis of compartment-specific T_2 values in WM.
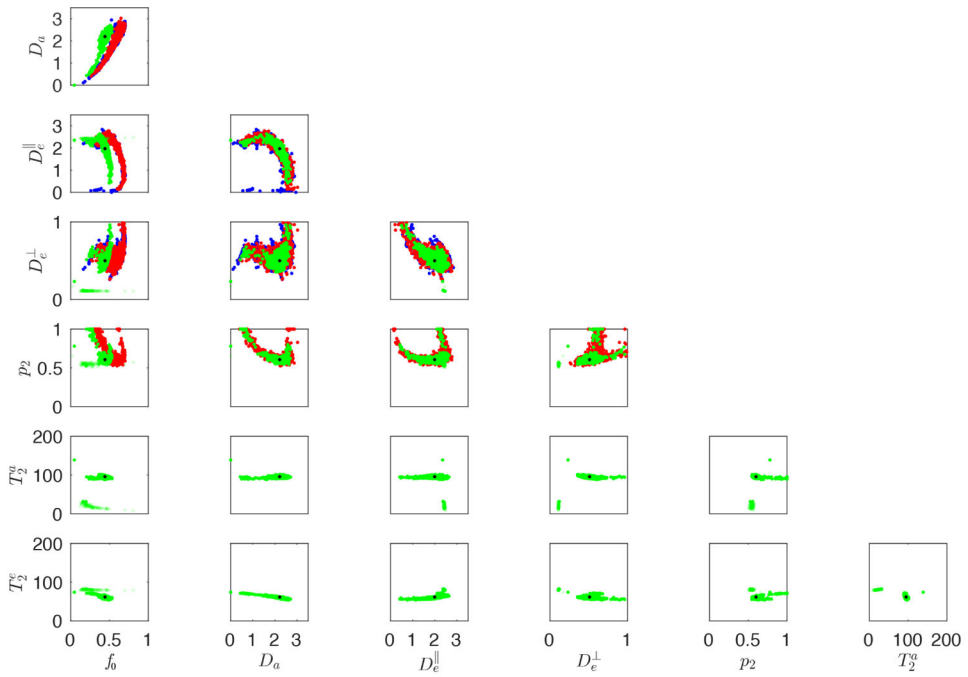
Figure 2.
Simulations: Scatter plots between all estimated parameters using rotational invariants K_0 (blue), $K_{0,2}$ (red), and TEdDI (green) are shown. The black dots indicate the ground truth values. TEdDI still results in multiple families of solutions. However, only one cluster of solutions is biophysically plausible and the T_2 values are the best discriminator. Spurious correlations between different parameters decrease in comparison to just using K_0 and $K_{0,2}$. The compartmental T_2 values are estimated with high accuracy and precision if non-plausible solutions are ignored.
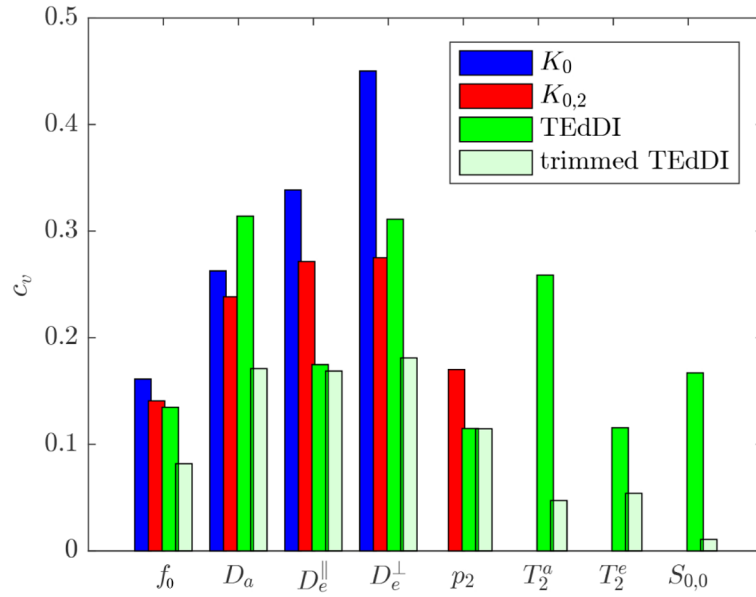
Figure 3.
Simulations: The coefficient of variation, c_v, is shown for the model parameters estimated using K_0 (blue), $K_{0,2}$ (red), and TEdDI (green). TEdDI shows similar or improved precision, especially after removing the biophysically implausible solutions based on the T_2 values (trimmed TEdDI). The compartmental T_2 values can be estimated with high precision.
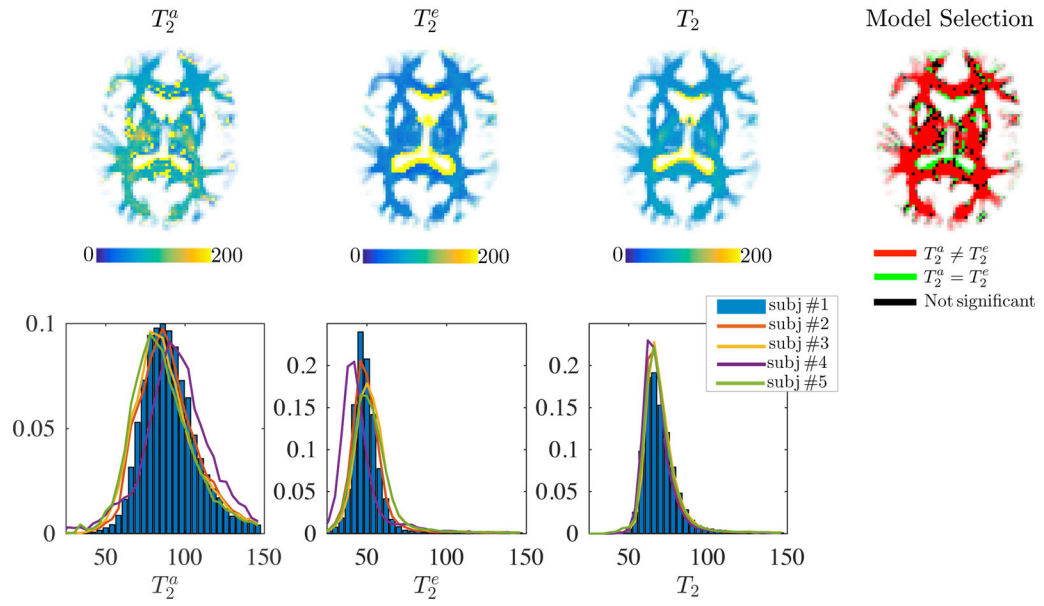
Figure 4.

Maps of T_2^a, T_2^e, and T_2 for subject #1 (top) and the associated T_2-distribution for all WM voxels, for all subjects (bottom). The corrected Akaike information criterion shows that unconstrained TEdDI provides a significantly better fit to the data in comparison to constrained version for which $T_2 \equiv T_2^a \equiv T_2^e$ (top right). Generally, $T_2^a > T_2^e$ and the difference is ROI specific. Partial voluming with cerebrospinal fluid (CSF) that is characterized by high T_2 render the two-compartment model, Eq. [2], inaccurate around e.g. the CC/CSF border.
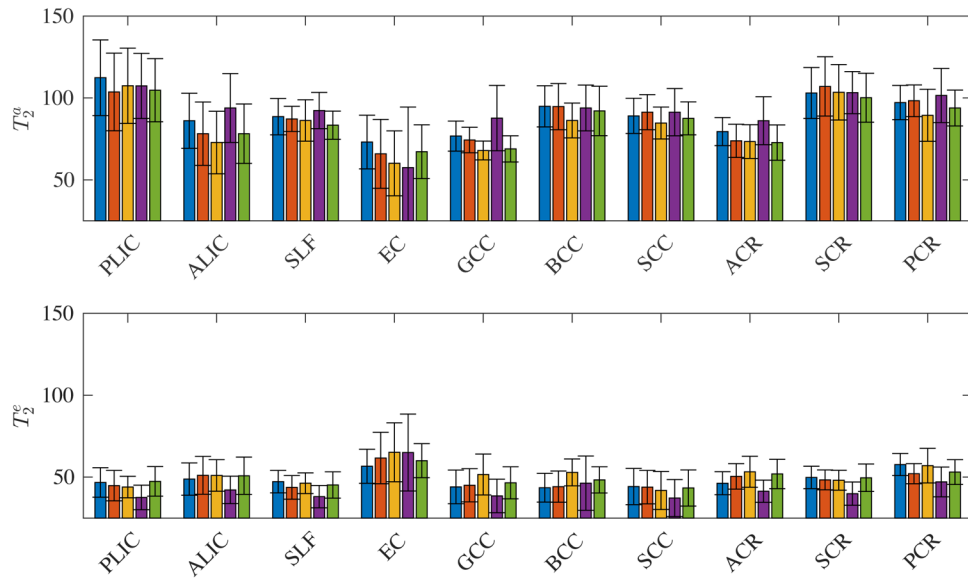
Figure 5.
The median (bar) and standard deviation (error bar) of the compartmental T_2 values for different major WM ROIs for each subject (different colors). The inter-subject differences are smaller than the inter-ROI and inter-compartment differences.
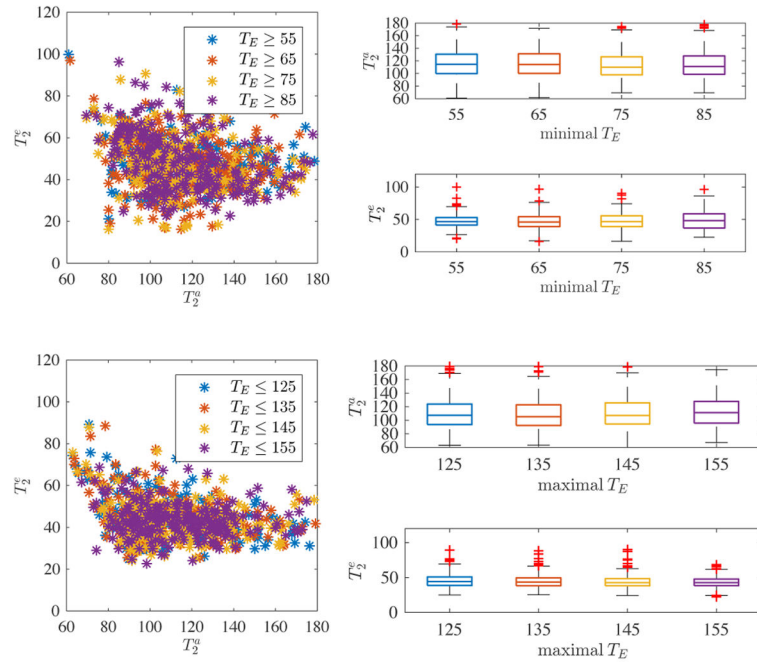
Figure 6.

Scatter plot for PLIC and one subject between the compartmental T_2's for different subsets of the data, whereby we varied minimal (top) and maximal (bottom) T_E included in the fitting. The associated box plots show a lack of trends by varying the analyzed T_E range. From this, we conclude that myelin water and intra/extra-axonal water exchange is likely not to interfere with the estimation of the T_2's.
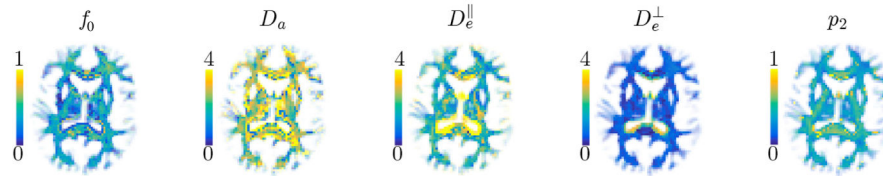
Figure 7.
Maps of diffusion model parameters. Partial volume effects with the CSF introduce biases in the estimation of model parameters. The precision of the maps and presence of outliers indicates the need for an additional, orthogonal measurement, or, maybe, the use of higher *b*-values.
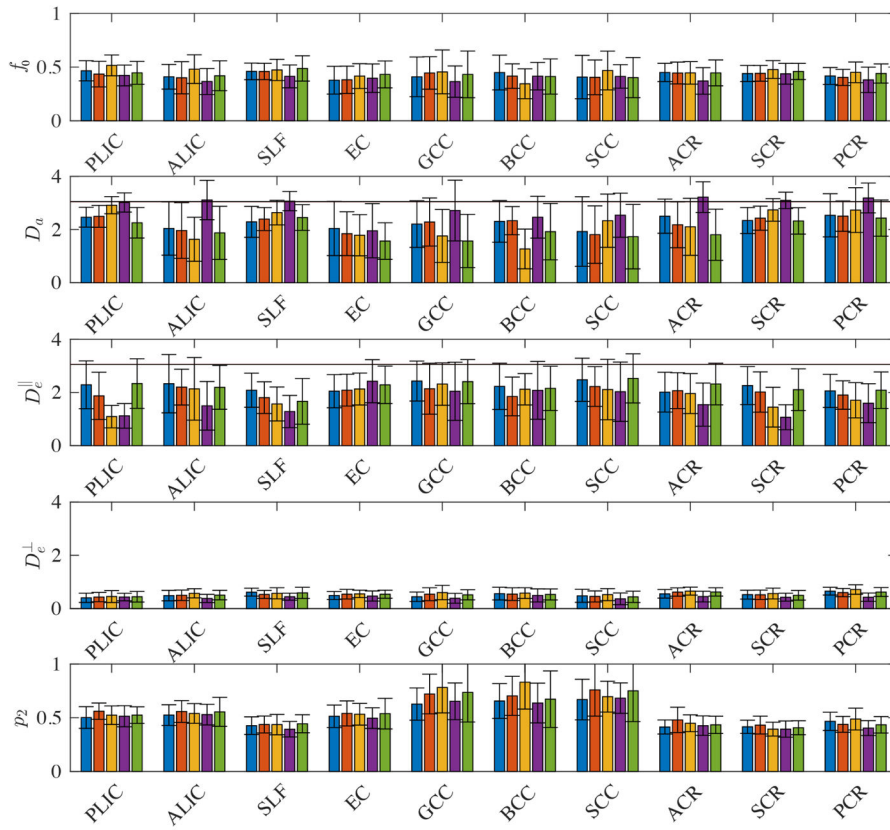
Figure 8.
The median (bar) and standard deviation (error bar) of the diffusion parameters for different major WM ROIs for each subject (different colors). Free diffusion at body temperature is indicated by the black horizontal lines.